Report Documentation Page

1. REPORT DATE **MAR 2003**	2. REPORT TYPE	3. DATES COVERED **00-00-2003 to 00-00-2003**
4. TITLE AND SUBTITLE **Very-long wave ternary antimonide superlattice photodiode with 21 um cutoff**		5a. CONTRACT NUMBER
		5b. GRANT NUMBER
		5c. PROGRAM ELEMENT NUMBER
6. AUTHOR(S)		5d. PROJECT NUMBER
		5e. TASK NUMBER
		5f. WORK UNIT NUMBER
7. PERFORMING ORGANIZATION NAME(S) AND ADDRESS(ES) **Naval Research Laboratory,4555 Overlook Avenue SW,Washington,DC,20375**		8. PERFORMING ORGANIZATION REPORT NUMBER
9. SPONSORING/MONITORING AGENCY NAME(S) AND ADDRESS(ES)		10. SPONSOR/MONITOR'S ACRONYM(S)
		11. SPONSOR/MONITOR'S REPORT NUMBER(S)

12. DISTRIBUTION/AVAILABILITY STATEMENT **Approved for public release; distribution unlimited**

13. SUPPLEMENTARY NOTES

14. ABSTRACT

15. SUBJECT TERMS

16. SECURITY CLASSIFICATION OF:			17. LIMITATION OF ABSTRACT	18. NUMBER OF PAGES	19a. NAME OF RESPONSIBLE PERSON
a. REPORT **unclassified**	b. ABSTRACT **unclassified**	c. THIS PAGE **unclassified**	**Same as Report (SAR)**	**3**	

Very-long wave ternary antimonide superlattice photodiode with 21 μm cutoff

E. H. Aifer,[a)] E. M. Jackson,[b)] G. Boishin,[c)] L. J. Whitman, I. Vurgaftman, J. R. Meyer, J. C. Culbertson, and B. R. Bennett
Naval Research Laboratory, Washington, DC 20375

We describe a ternary antimonide superlattice photodiode with a 21 μm cutoff wavelength. The active region consists of 150 periods of 10 monolayers (MLs) of In$_{0.07}$Ga$_{0.93}$Sb and 19 MLs of InAs with InSb-like interfacial bonds. The device has a detectivity of 3×10^9 cm$\sqrt{\text{Hz}}$/W, dynamic impedance-area product of 0.18 Ω cm^2, and peak external quantum efficiency of 3% at 40 K. X-ray diffraction and cross-sectional scanning tunneling microscopy show the structure to have a high degree of order with abrupt interfaces. A simulation of the absorption spectrum effectively reproduces the observed spectrum. © *2003 American Institute of Physics.*
[DOI: 10.1063/1.1584518]

Currently, the two leading very-long wave infrared (VLWIR) focal plane array technologies for space-based detection employ blocked impurity band silicon (Si:BIB) and mercury–cadmium–telluride (MCT), both of which have significant drawbacks. High thermal generation rates in the extrinsic Si:BIBs limit their operating temperatures to $\approx$10 K,[1] while MCT-based photovoltaics are limited to the short end of the VLWIR by band-to-band tunneling, which grows exponentially as the energy gap decreases.

Photodiodes based on antimonide superlattices (ASLs) offer a promising alternative to these systems. As proposed by Smith and Mailhiot[2] and grown by Chow *et al.*,[3] superlattices constructed of alternating layers of type-II aligned In$_x$Ga$_{1-x}$Sb and InAs would have a metallic band structure but for quantum confinement effects that produce an arbitrarily small positive band gap that increases as a function of decreasing superlattice period. While the peaks of the electron and hole wave functions are located in the InAs and ternary layer, respectively, degradation in the wave function overlap can be mitigated to the extent that the IR absorption coefficients are comparable to those in bulk MCT. This is accomplished at a given wavelength by minimizing the superlattice period, which can be achieved by increasing the alloying of the In$_x$Ga$_{1-x}$Sb layer, reducing confinement effects.[2] A key advantage over MCT in VLWIR applications arises from the significantly heavier ASL electron effective mass that greatly reduces band-to-band tunneling.[2] Second, as observed by Youngdale *et al.*,[4] Auger recombination rates, relative to bulk MCT, are strongly suppressed due to the large splitting of the light and heavy hole bands in the superlattice band structure. Supporting evidence has been provided by steadily increasing detectivities (D^*) and cutoff wavelengths (λ_{co}) of ASL photodiodes, with Wei *et al.*[5] recently reporting a binary GaSb/InAs photodiodes with $\lambda_{co}>30$ μm. However, in the 8–12 μm range, ternary ASLs display the highest D^*'s, which now rival those of MCT.[6]

Here, we describe a ternary ASL photodiode with a 21 μm cutoff wavelength. The introduction of ternaries with variable In mole fraction x substantially expands the opportunities for the improved performance of ASLs in the VLWIR, since the strain compensation can be decoupled from other design optimizations and the incorporation of In into the GaSb hole wells allows for longer λ_{co} in shorter-period structures with enhanced optical matrix elements.

The photodiodes in this study were grown in a Riber Compact 21T molecular-beam epitaxy (MBE) system equipped with valved As and Sb crackers producing diatomic group-V flux. Dual In sources permit x in the In$_x$Ga$_{1-x}$Sb layers to be controlled independently of the InAs growth rate. Growth rates were calibrated by monitoring intensity oscillations in the reflected high-energy electron diffraction (RHEED) patterns during the growth of GaSb and InAs under excess group-V flux. The InGaSb layers were nominally grown at 1 ML/s at a V:III flux ratio of about 1.5, while the InAs layers were grown at 0.5 ML/s with a flux ratio of about 2. The alloy composition x was controlled by setting the Ga growth rate to 0.92 ML/s and the second In source to a rate of 0.08 ML/s. Hall measurements on doped GaAs films grown on semi-insulating GaAs substrates were used to calibrate p-type (Be) and n-type (Si–InAs) doping. Absolute substrate temperature was referenced to the points at which oxide desorption and the (1×5)-to-(1×3) surface reconstruction transition were detected with RHEED.[7]

The n-on-p superlattice photodiodes were grown on an unintentionally doped, GaSb (001) substrate with a net p-type doping of $1-2\times10^{17}$ cm^{-3}. After oxide desorption, a 0.5 μm thick p^+-GaSb buffer/contact layer ($\sim10^{18}$ cm^{-3}) was grown with the substrate kept at 495 °C to suppress the formation of dilatory pyramidal defects.[8] The substrate temperature was then lowered to 400 °C for growth of the 150 period superlattice, which had a nominal period structure of 10 monolayers (MLs) of In$_x$Ga$_{1-x}$Sb on 18 ML InAs with 1 ML of InSb-like interfacial bonds[9,10] (29 MLs total). Next, 1 μm of a lightly p-doped superlattice ($\sim5\times10^{15}$ cm^{-3}) was grown, followed by 300 nm of n^+ superlattice capped with a 20 nm thick InAs n^+-contact layer doped $\sim10^{18}$ cm^{-3}.

Large, unpassivated mesa diodes were fabricated in a

[a)]Electronic mail: aifer@estd.nrl.navy.mil
[b)]Also at: SFA Incorporated, Largo, MD 20774.
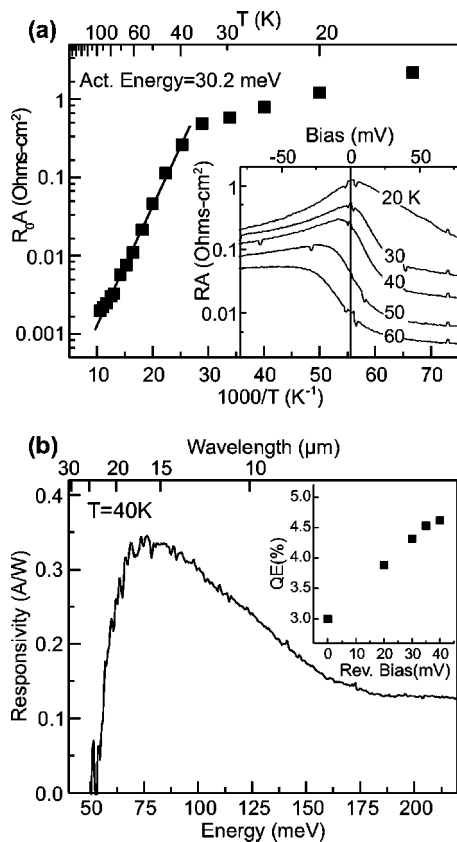[c)]Also at: NOVA Research Incorporated, Alexandria, VA 22308.

FIG. 1. (a) The dynamic impedance-area product, R_0A, as a function of temperature for a n-on-p photodiode with a top contact covering the 200 μm diameter, circular mesa. Bias dependence of RA is shown in the inset. (b) The absolute power responsivity vs photon energy for a 400 μm circular diode, with cutoff wavelength of 21 μm (50% peak) at 40 K. The inset shows the quantum efficiency of the device as a function of reverse bias.

simple two-step process. First, mesas were defined by wet etching in a solution of citric acid, hydrogen peroxide, phosphoric acid, and deionized water. The devices were then completed with the patterning and deposition of Ti/Pt/Au n- and p-type ohmic contacts. Linear and circular transmission line measurements indicated contact resistivities in the 10^{-6} Ω cm^2 range for both contact types.

The relative IR spectral responsivity was measured by diverting the interferometer output of a Nicolet Magna-IR 750 Fourier transform infrared spectrometer onto the sample through a KRS-5 cryostat window. Because the cutoff for the device approached the 27 μm limit of the mid-IR beamsplitter (Ge on KBR substrate), the spectral line shape was also recorded using a far-IR silicon beamsplitter, with similar results. The absolute responsivity ($\Re$) was determined using black-body measurements with a spectrally calibrated Infrared Industries IR-463 source. Measurements of the detector current as a function of black-body aperture diameter confirmed the absence of spurious IR coupling. Black-body measurements were made through a 10–14 μm bandpass filter with a 27° field of view. Note that our reported $\Re$ and quantum efficiency (η) values do not correct for the reflection of $\approx$30%.

The dynamic impedance-area product, RA (R_0A at zero bias), is displayed as a function of temperature in Fig. 1(a) for a 200 μm circular device with a top contact covering the mesa. Activated behavior is evident down to $\approx$40 K, with an activation energy E_A=30.2 meV. The inset shows how RA

depends on temperature under bias. Carrier freeze out (in the substrate) is evident between 20 and 30 K, where RA remains high under forward bias, while the premature saturation with reverse bias below 40 K indicates leakage processes. The absolute responsivity versus photon energy is shown in Fig. 1(b) for a 400 μm circular device with a 160 μm diameter contact to allow optical access. The cutoff for this device (50% peak responsivity) occurs just below 60 meV, or 21 μm. However, the peak responsivity and quantum efficiency are relatively low, at 0.35 A/W and 3%, respectively. The responsivity can be modestly improved under reverse bias, as shown in the inset of Fig. 1(b), with a maximum increase of 50% at $V=-40$ mV. With an R_0A of 0.18 ohm cm^2, this device has a Johnson noise limited D^* of 3×10^9 cm$\sqrt{}$Hz/W at 40 K and zero bias. Note that the activation energy is approximately half of the energy gap, indicating that the diode operates in a generation-recombination-limited mode, with R_0A proportional to the intrinsic carrier density, and therefore never reaches the diffusion-limited regime.

X-ray diffraction (XRD) and cross-sectional scanning tunneling microscopy (X-STM) measurements were performed to determine the actual superlattice period and strain, and to examine both the long- and short-range order within the layers. XRD spectra were obtained using a Bede QC1a double-crystal diffractometer, and then compared with dynamical XRD simulations generated with Bede's RADS software to determine the structural parameters. From the XRD measurements, shown in Fig. 2(a), the period and relaxed average lattice constant were found to be 90.60 and 6.093 Å, respectively, equivalent to 29.75 ML of III-V growth, with a -0.04% mismatch to the GaSb substrate. The diffraction peaks are extremely narrow, with a full width at half maxima of 23 arc s for both the substrate and the zeroth-order satellites, indicating a high degree of long-range order.

The XRD spectrum was simulated using a range of In alloy fractions ($x=6\%$ to 9%), and InGaSb and InAs film thicknesses that satisfied the observed period and strain assuming InSb-like interfaces. The measured spectral peak positions and amplitudes were well reproduced by the equivalent of either 9.9 ML In$_{0.07}$Ga$_{0.93}$Sb/18.8 ML InAs, as shown in Fig. 2(a), or 9.4 ML In$_{0.08}$Ga$_{0.92}$Sb/19.3 ML InAs.

The nanometer-scale structure of the superlattice was characterized by X-STM, with the wafer cleaved in an ultra-high vacuum to expose a {110} surface that presents a cross-sectional view through a single lattice plane.[11,12] Images of the ($1\bar{1}0$) surface, shown in Fig. 2, were acquired with filled electronic states, revealing every-other group-V lattice plane within the structure in cross section. The InGaSb layers appear $\sim$0.1 nm higher ("brighter") than the InAs layers, due primarily to differences in the surface electron density of states.[12] Consistent with the XRD, the superlattice exhibits excellent long-range order [Fig. 2(b)], with no evidence of lateral modulations, alloy segregation, or accumulating roughness during growth. At the atomic scale [Fig. 2(c)], the interfaces appear smooth and abrupt, with only occasional growth steps observed along the interfaces and any disorder associated with interfacial bond formation confined within $\sim$1 ML. Enumerating the apparent Sb and As rows per period, we estimate 11 MLs of InGaSb+InSb plus 18 or 19

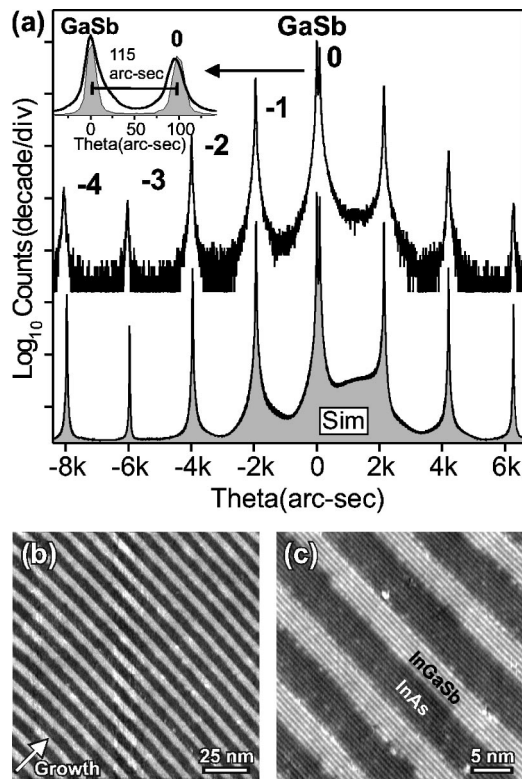Appl. Phys. Lett., Vol. 82, No. 25, 23 June 2003

Aifer *et al.* 4413

FIG. 2. (a) XRD analysis of the superlattice. The measured (top) and simulated (bottom) spectra were used to determine the thickness and composition of the superlattice as the equivalent of 9.9 ML $In_{0.07}Ga_{0.93}Sb$/18.8 ML InAs with a plane of InSb bonds at each interface. (b) and (c) Filled-state X-STM images of the superlattice with fields of view of 150 nm and 35 nm, respectively.

MLs of InAs. There is a relative uncertainty of ± 1 ML because only every-other growth layer is seen, and steps on the growth surface occasionally shift the apparent position of an interface by 1 ML.[11]

We find that the main spectral features of this device are well described by a $\mathbf{k \cdot p}$ simulation of the absorption coefficient based on the observed structure of the active region. The experimental absorption spectrum, $\alpha_R(\lambda)$ shown in Fig. 3, was extracted from the measured spectral responsivity by first deriving the external quantum efficiency spectrum,

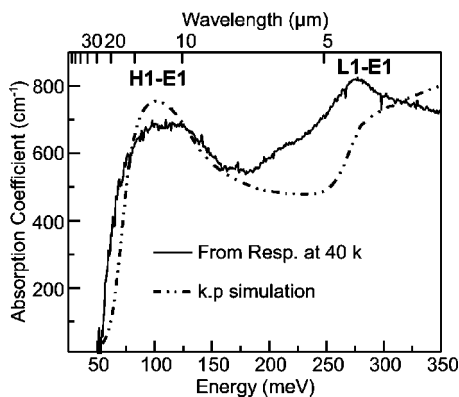$$\eta(\lambda) = 1/e \frac{hc}{\lambda} \Re(\lambda),$$

FIG. 3. The measured and simulated absorption coefficients. The measured spectrum was extracted from the spectral responsivity in Fig. 1(b). The simulated spectrum was modeled using an eight-band finite-element $\mathbf{k \cdot p}$ calculation.

where e is the electron charge, h is Planck's constant, and c is the speed of light. The absorption spectrum was then obtained from the relation

$$\alpha_R(\lambda) = -\frac{1}{d} \ln\left[1 - \frac{\eta(\lambda)}{(1-R)\chi}\right].$$

Here, d is the thickness of the lightly p-doped superlattice absorbing region (1 μm), R is the reflectivity, and the (unknown) collection efficiency χ represents the fraction of optically generated electron–hole pairs that contribute to the photocurrent.

The simulated absorption coefficient was modeled using an eight-band, finite-element $\mathbf{k \cdot p}$ calculation of the superlattice electronic states,[13] assuming Gaussian inhomogeneous linewidths of 5 meV. Scaling the experimental data using $\chi \approx 0.65$, the absorption coefficient is well simulated with an In alloy fraction in the 7%–8% range (Fig. 3). Although the calculated spectrum is weighted more heavily toward the band edge, the energy positions of the main transitions from the highest heavy-hole (H1) and light-hole (L1) subbands to the lowest electron subband (E1) agree well.

To summarize, we have described a ternary ASL photodiode with a cutoff wavelength of 21 μm. The temperature dependence of R_0A shows the diode to be generation-recombination limited above 40 K. The detectivity $D^* = 3 \times 10^9$ cm$\sqrt{Hz}$/W occurs with a peak quantum efficiency of 3%, in the Johnson noise limit. The superlattice was characterized by XRD and X-STM, showing that the structure has a high degree of long- and short-range order and abrupt interfaces. The main optical transitions of the device are well explained by a simulation of the absorption coefficient based on the structure of the active region, and an overall collection efficiency of ≈ 0.65.

[1] M. A. Kinch, J. Electron. Mater. **29**, 809 (2000).
[2] D. L. Smith and C. Mailhiot, J. Appl. Phys. **62**, 2545 (1987).
[3] D. H. Chow, R. H. Miles, J. R. Soderstrom, and T. C. McGill, Appl. Phys. Lett. **56**, 1418 (1990).
[4] E. R. Youngdale, J. R. Meyer, C. A. Hoffman, F. J. Bartoli, C. H. Grein, P. M. Young, H. Ehrenreich, R. H. Miles, and D. H. Chow, Appl. Phys. Lett. **64**, 3160 (1994).
[5] Y. Wei, A. Gin, M. Razeghi, and G. J. Brown, Appl. Phys. Lett. **81**, 3675 (2002).
[6] F. Fuchs, U. Weimer, W. Pletschen, J. Schmitz, E. Ahlswede, M. Walther, J. Wagner, and P. Koidl, Appl. Phys. Lett. **71**, 3251 (1997); Q. K. Yang, F. Fuchs, J. Schmitz, and W. Pletschen, *ibid.* **81**, 4757 (2002).
[7] A. S. Bracker, M. J. Yang, B. R. Bennett, J. C. Culbertson, and W. J. Moore, J. Cryst. Growth **220**, 384 (2000).
[8] E. H. Aifer, E. M. Jackson, B. R. Bennett, I. Vurgaftman, J. R. Meyer, and G. G. Jernigan, Mater. Res. Soc. Symp. Proc. **722**, K10.1 (2002).
[9] D. H. Chow, R. H. Miles, and A. T. Hunter, J. Vac. Sci. Technol. B **10**, 888 (1992).
[10] J. R. Waterman, B. V. Shanabrook, R. J. Wagner, M. J. Yang, J. L. Davis, and J. P. Omaggio, Semicond. Sci. Technol. **8**, s106 (1993).
[11] B. Z. Nosho, W. Barvosa-Carter, M. J. Yang, B. R. Bennett, and L. J. Whitman, Surf. Sci. **465**, 361 (2000).
[12] S. G. Kim, S. C. Erwin, B. Z. Nosho, and L. J. Whitman, Phys. Rev. B **67**, 121306(R) (2003).
[13] L. R. Ram-Mohan and J. R. Meyer, J. Nonlinear Opt. Phys. Mater. **4**, 191 (1995).